

Design and Electromagnetic Loss Analysis of High Speed Permanent Magnet Synchronous Motor for an Air Compressor

Xiaojun Ren^{*}, Ming Feng, and Jinliang Liu

Abstract—Air compressors are widely used in various industrial fields. The motor of air compressor requires high power and high speed. This paper focuses on the structural design and loss analysis method of high-speed permanent magnet synchronous motor in air compressor. The structure of motor is designed. The key parameters are calculated. The influence of structural parameters on motor loss is analyzed. The analytical and design results are verified by finite element method (FEM). Finally, the prototype of motor has been manufactured. The performance of the motor is verified on the prototype.

1. INTRODUCTION

Nowadays, the demand for air compressor in industrial production process will continue to increase along with the development of manufacture automation. When the air compressor works normally, the compressed air generates pressure [1, 2]. Motor is one of the core components of an air compressor. Due to the advantages of low noise, high efficiency, high power density, and good speed regulation performance, permanent magnet synchronous motor (PMSM) is widely used in air compressors, electric vehicles, numerical control machines, and other fields [3–7].

As for the motor system, design and control are most important aspects [8, 9]. There are some important factors for high-speed motor design, such as critical speed, stress of rotor, eddy current loss of the rotor, permanent magnet (PM), and retaining sleeve [10–13]. The traditional design method for motor is to obtain the main structure dimensions from the formulas in the design manual. Calculation of the formulas is often based on the magnetic circuit method [14]. As the magnetic circuit model is simplified by the magnetic field, the accurate magnetic field distributions cannot be obtained in this way [15]. Therefore, the value obtained by the magnetic circuit formula usually needs further optimization. In order to improve the motor's performance, more and more researchers adopt the combination method of magnetic circuit and field analysis to design motor [16]. As for optimization of the motor, some researchers optimize the motor by a certain optimization algorithm based on a lumped parameter model. The optimization results can be verified by the finite element method [17, 18]. Meanwhile, other researchers who think the lumped parameter model is not reliable enough directly chose the finite element model for optimization [19]. In literature [20], the motor was optimized by dividing variables into control variables and design variables.

In this paper, a design and loss analysis method of high speed permanent magnet synchronous motor for an air compressor is studied. Firstly, the structure of the motor is designed. Then the key structural parameters are calculated theoretically. The structural parameters affecting the loss are optimized. The electromagnetic characteristics and loss of the motor are simulated by finite element method. Finally, the main performance of the motor is tested on the prototype platform.

Received 1 April 2022, Accepted 25 May 2022, Scheduled 14 June 2022

* Corresponding author: Xiaojun Ren (renxiaojun@ustb.edu.cn).

The authors are with the School of Mechanical Engineering, Beijing University of Science and Technology, Beijing, China.

2. STRUCTURE PARAMETERS DESIGN

The cross section of the motor structure is shown in Fig. 1. It can be seen from Fig. 1 that a pair of magnetic steels are tightly surrounded outside the rotor core. The sheath is assembled outside the magnetic steel.

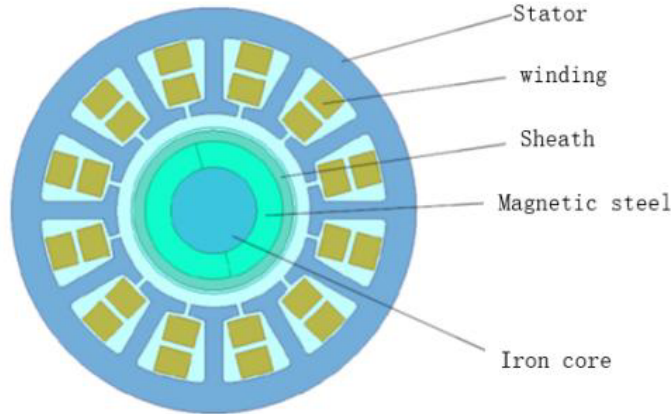


Figure 1. Structure of motor.

The structure design of high-speed permanent magnet synchronous motor mainly includes the selection of pole slot ratio, motor size, rotor structure, stator and rotor materials, winding mode, etc.

2.1. Determination of the Number of Poles

The number of poles and speed of permanent magnet synchronous motor determine the electromagnetic alternating frequency of the motor, and the electromagnetic alternating frequency affects the iron loss in the stator. Therefore, in order to reduce the stator iron loss, it is necessary to reduce the magnetic field alternating frequency. The electromagnetic frequency of the motor f can be calculated as follows

$$f = \frac{np}{60} \quad (1)$$

where n is the rotation speed; p is the number of poles.

It can be seen that the higher the number of poles of the motor is, the higher the electromagnetic alternating frequency is, and the higher stator iron loss will be produced. In order to reduce the loss and processing difficulty, the motor design of the project adopts one pole structure. Here we choose $p = 1$.

2.2. Determination of the Number of Slots

Due to the small size of the motor in this subject, if the 24 slot structure is adopted, the stator teeth will be narrow, and the slot will be small, which increases the difficulty of processing the stator lamination and winding off-line. To sum up, the motor of this subject adopts 12 slot structure.

2.3. Determination of Rotor Outer Diameter

Permanent magnet motor rotor rotation produces rotating magnetic field. Under the condition of the same winding, the larger the outer diameter of the rotor is, the greater the magnetic flux it can provide, and the greater the no-load back EMF coefficient and torque coefficient of the motor are. However, a large outer diameter of the rotor will lead to a large linear speed on the rotor surface, resulting in a large centrifugal force. For permanent magnet materials with low tensile strength, a large centrifugal force will lead to insufficient rotor strength, even magnetic steel fracture and motor failure. At the

same time, the larger outer diameter of the rotor increases the inertia of the rotor, which will lead to the deterioration of the dynamic performance of the rotor and affect the starting response and speed regulation performance of the motor.

According to the project requirements, the motor speed is 90krpm. In order to ensure both rotor strength and motor power density, the linear speed on the outer surface of the rotor is 170 m/s. Therefore, the outer diameter of rotor can be calculated as

$$D_{ro} = \frac{60v}{n\pi} \quad (2)$$

where D_{ro} is the outer diameter of rotor; n is the motor speed, in rpm; v is the linear speed of the outer surface of the rotor.

2.4. Inner Diameter of Stator

The largest part of the reluctance in the motor is the air gap. The air gap length is determined by the stator inner diameter and rotor outer diameter of the motor. The larger the air gap length is, the greater the magnetic resistance is, the lower the air gap magnetic density is, and the lower the power density of the motor at the same output power is. Then the volume of the motor will increase, and the manufacturing cost of the motor will increase too. On the contrary, if the air gap length is too small, the magnetic resistance is reduced; the air gap magnetic density is increased; and the local magnetic density of the stator will be higher. As a result, the loss will be increased, and the motor temperature rise will be increased, which will not only reduce the working efficiency of the motor, but also lead to non demagnetization of the magnetic steel and motor failure. Therefore, the length of the air gap cannot be too large or too small.

Due to the high-speed rotation of the rotor, in order to ensure the strength of the rotor magnetic steel, it is necessary to install the magnetic steel sheath. On overall consideration, stator inner diameter can be obtained by the following equation.

$$D_{sin} = D_{ro} + L_{sh} + L_{ag} \quad (3)$$

where D_{sin} is the Inner diameter of stator; D_{ro} is the outer diameter of rotor; L_{sh} is the radial length of sheath; L_{ag} is the length of air gap.

2.5. Stator Length

The length of the stator is another major dimension of the motor. The general rough calculation of stator length usually adopts the following equation

$$L_{st} = \frac{6.1 \times 10^7 P}{D_{sin}^2 \alpha AB_{\delta}} \quad (4)$$

where L_{st} represents the length of stator; D_{sin} is the Inner diameter of stator; α is pole arc coefficient; A is the number of ampere conductors per unit length along the circumference of the armature; B_{δ} is the average air gap magnetic density.

3. LOSS ANALYSIS AND PARAMETERS OPTIMIZATION DESIGN

Permanent magnet synchronous high-speed and high-power motor in an air compressor requires high efficiency, that is, the loss of the motor is small during operation. Therefore, it is necessary to analyze the mechanism of various motor losses and accurately calculate various losses under different working conditions.

There are two main factors affecting motor loss. The first factor is the internal structure design including structural parameters and material properties. Due to the different external power supply modes of the motor, the magnetic density distribution inside the motor changes, which results in the loss change. The loss of a motor is mainly divided into four parts, including stator winding copper loss, stator iron loss, rotor eddy current loss, and mechanical loss. In this paper, high speed and high power motor focuses on copper loss, stator iron loss, and rotor eddy current loss.

(1) Influence of PM thickness on loss

A magnetic steel is installed on the rotor of the permanent magnet synchronous motor. The rotating magnetic field generated after the stator coil is energized interacts with the magnetic field generated by the rotor magnetic steel to drive the rotor to rotate. The diameter of the rotor has been designed as 39 mm, which is fixed. According to the actual processing requirements of the project, PM thickness varies from 3 to 5 mm. Fig. 2 shows the influence of PM thickness on loss.

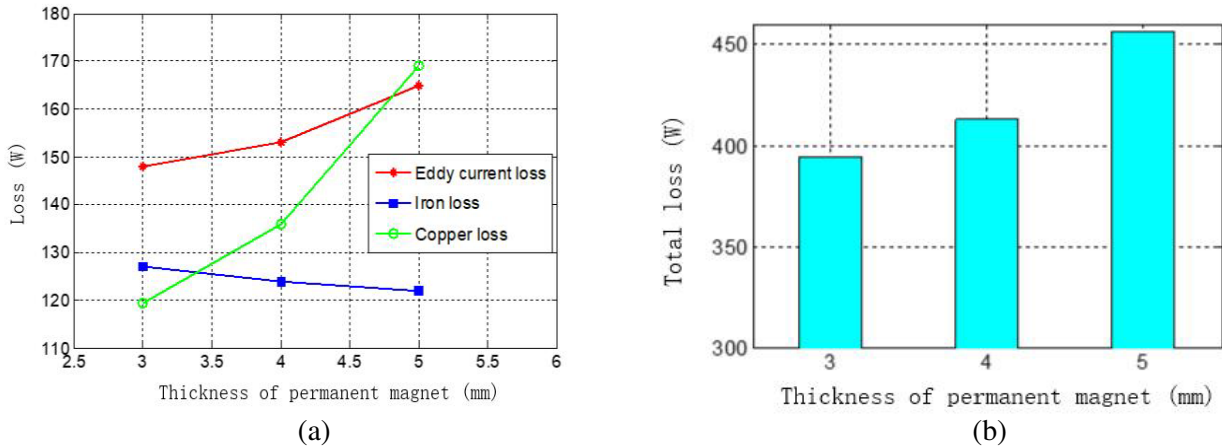


Figure 2. Influence of PM thickness on loss. (a) Influence chart on various losses. (b) Influence chart on total losses.

It can be seen from Fig. 2(a) that the eddy current loss decreases with the decrease of the thickness of the magnetic steel. The main reason is that the air gap flux density decreases with the decrease of steel thickness. With the decrease of the thickness of magnetic steel, the copper loss increases. This is because the back EMF decreases, and the current increases when the thickness of the magnetic steel decreases. With the decrease of the thickness of magnetic steel, the iron loss changes little. It can be seen from Fig. 2(b) that with the decrease of the thickness of magnetic steel, the total loss increases. This is because the increase of copper loss is much less than that of eddy current loss.

(2) Influence of stator outer diameter on loss

Figure 3 shows the influence of stator outer diameter on loss. It can be seen from Fig. 3 that with the increase of outer diameter, eddy current loss decreases, and iron loss increases. Stator iron loss is

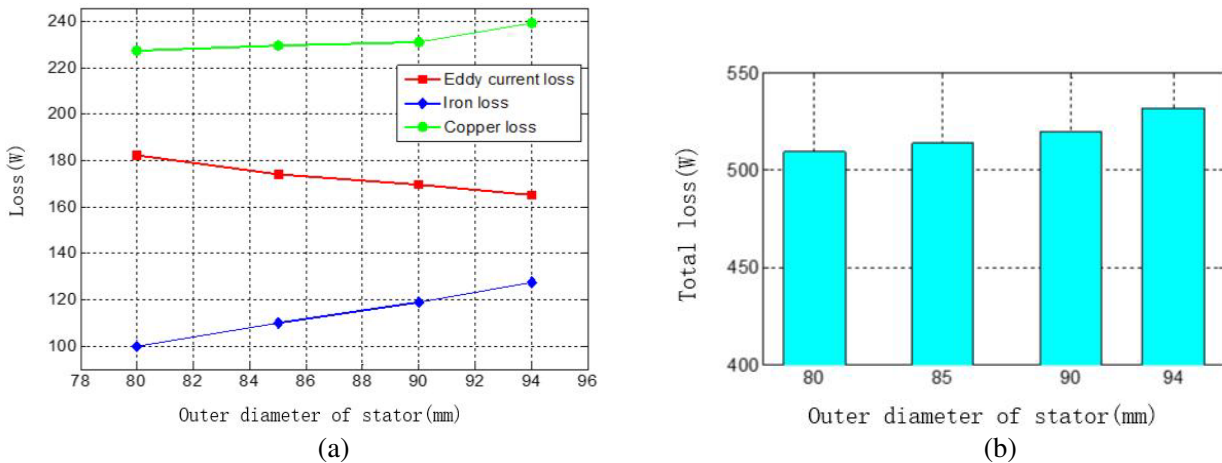


Figure 3. Influence of stator outer diameter on loss. (a) Influence chart on various losses. (b) Influence chart on total losses.

positively correlated with stator mass, magnetic density, and magnetic field alternating frequency. The stator volume increases, so the iron loss increases. Copper loss slightly increases, and the total loss increases.

(3) Influence of air gap length on loss

Figure 4 shows the influence of air gap length on loss. It can be seen from Fig. 4 that with the increase of air gap length, both of eddy current loss and iron loss decrease. However, copper loss increases. The total loss achieves the max value when length of the air gap is 11 mm. When length of the air gap is 15 mm, both the eddy current loss and total loss have the minimum values. Therefore, the optimal value of length of the air gap is designed as 15 mm in this paper.

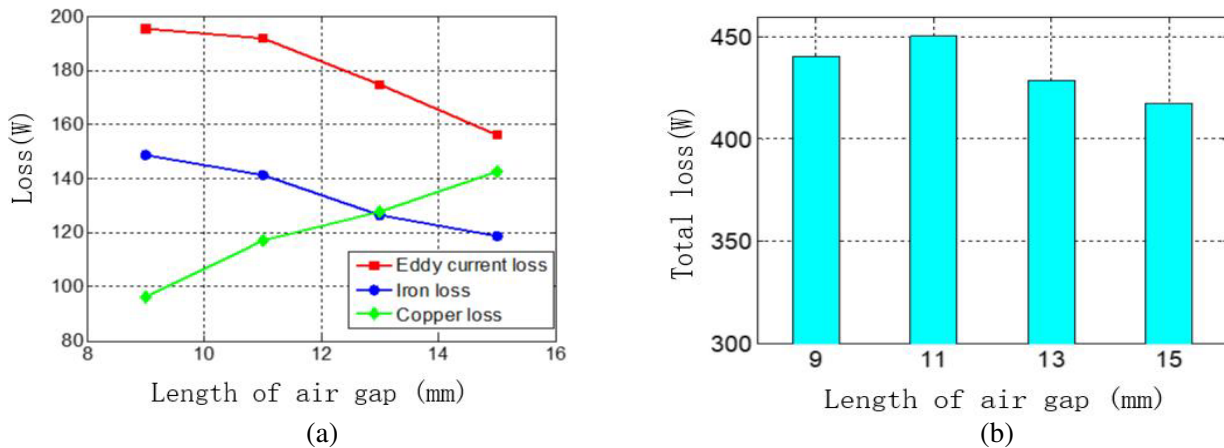


Figure 4. Influence of air gap length on loss. (a) Influence chart on various losses. (b) Influence chart on total losses.

(4) Influence of thickness of yoke on loss

Figure 5 shows the influence of thickness of yoke on loss. It can be seen from Fig. 5 that when the thickness of yoke changes from 7 mm to 9 mm, both copper loss and iron loss have a small decrease, while eddy current loss has a large increase. As a result, the total loss achieves the max value when the thickness of yoke is 9 mm. Considering each loss and total loss, the optimal value of thickness of yoke is 8 mm.

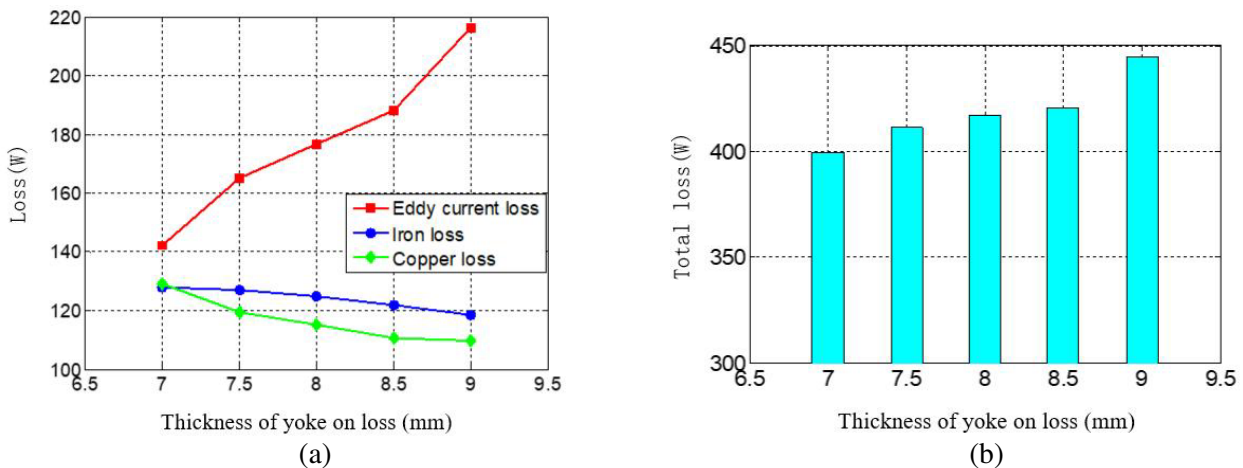


Figure 5. Influence of thickness of yoke on loss. (a) Influence chart on various losses. (b) Influence chart on total losses.

(5) Influence of tooth width of stator on loss

Figure 6 shows the influence of tooth width of stator on loss. It can be seen from Fig. 6 that when the thickness of yoke changes from 3 mm to 3.5 mm, both eddy current loss and iron loss increase, while copper loss decreases. As a result, the total loss has a small increase. However, when thickness of yoke changes from 3.5 mm to 5 mm, due to the large increase in the value of eddy current loss, the total loss increases greatly. Therefore, the optimal value of tooth width of stator was designed as 3.5 mm.

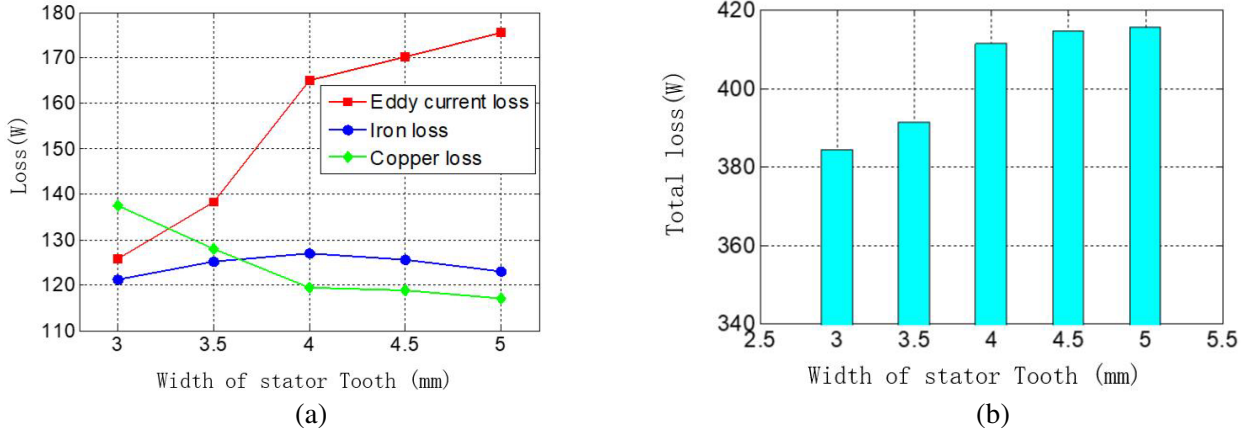


Figure 6. Influence of air gap length on loss. (a) Influence chart on various losses. (b) Influence chart on total losses.

Based on the previous calculation and optimization design, parameters of the motor by considering the comprehensive performance are listed in Table 1. The motor was designed as an 18 kW, 90000 rpm HSPMM.

Table 1. Parameters and design variables of HSPMM.

name	value
Outer diameter of stator	94 mm
Inner diameter of stator	45 mm
Outer diameter of magnetic steel	32 mm
Inner diameter of magnetic steel	20 mm
Outer diameter of sheath	37 mm
Core length	8 mm
Pitch	5
Number of parallel branches	2
Number of conductors per slot	10
Outer diameter of magnetic steel	42 mm

4. FEM SIMULATION

The main performances of the motor, including electromagnetic distribution, torque, and loss are calculated by FEM.

(1) Simulation of magnetic field distribution

The magnetic field distribution of motor by FEM simulation is shown in Fig. 7. It can be seen from Fig. 7(a) that the maximum magnetic induction intensity of stator teeth is 1.6 T, and the magnetic

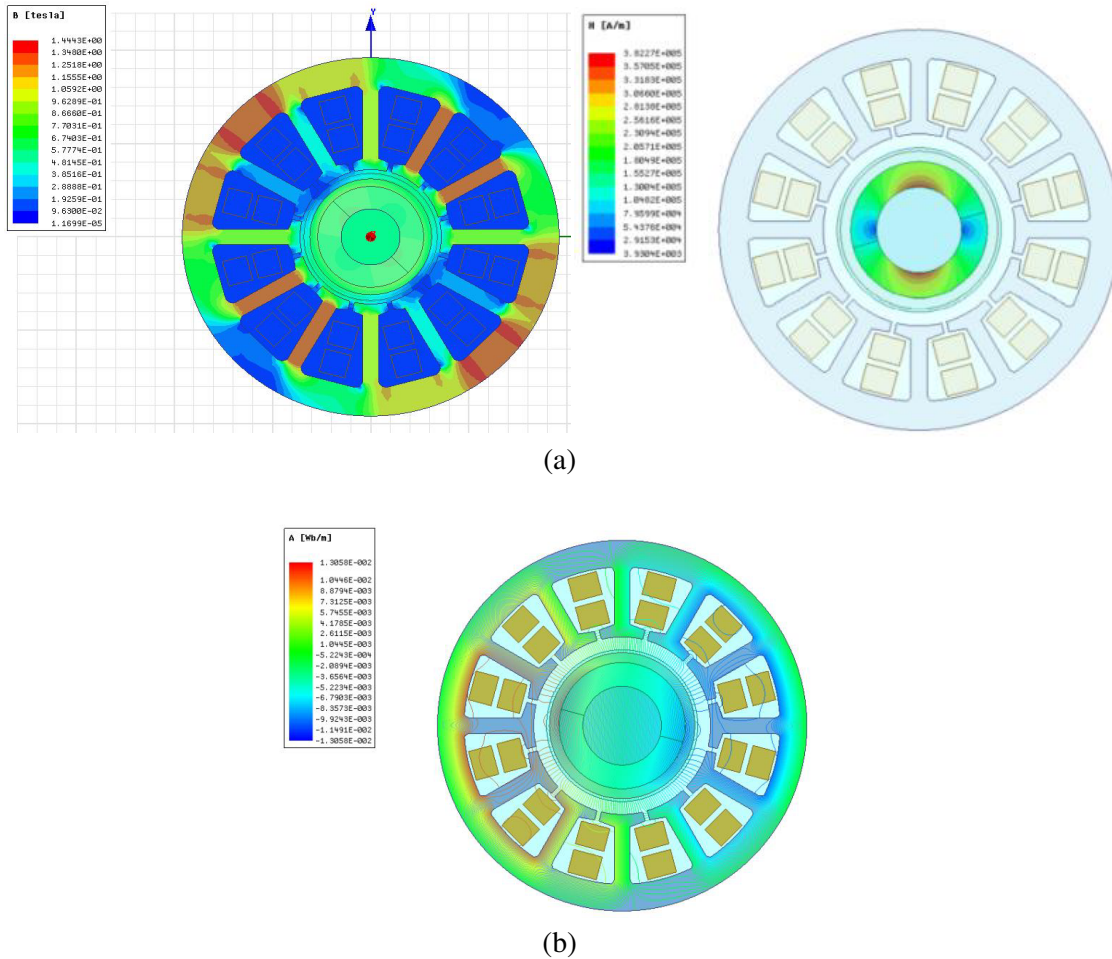


Figure 7. Simulation of magnetic field distribution. (a) Magnetic induction intensity stator and magnetic steel. (b) Magnetic flux lines.

induction intensity of stator yoke reaches 1.65 T, which does not exceed the magnetic saturation density of stator laminations. The maximum magnetic field intensity is 383 KA/m, which is far less than the demagnetization magnetic field intensity of 911 KA/m. It can be seen from the magnetic field line distribution of the motor in Fig. 7(b) that the magnetic flux leakage at the end is not obvious.

(2) Simulation of output torque

The three-phase current waveform of motor winding is shown in Fig. 8(a). It can be seen from Fig. 8 that the effective value of phase current is 85 A, and the peak value of phase current is 160 A. The output torque waveform of the motor at speed 9krpm when the control voltage is 235 V is shown in Fig. 8(b). It can be seen that the average output torque is 1.77 N·m, which meets the design requirements of the rated output torque of 1.7 N·m.

(3) Loss simulation

Motor losses mainly include copper loss, iron loss, and eddy current loss. The waveform of loss at speed 9krpm is shown in Fig. 9. It can be seen from Fig. 9(a) that the iron loss of the motor is 152 W. It can be seen from Fig. 4(b) that the eddy current loss is 143 W.

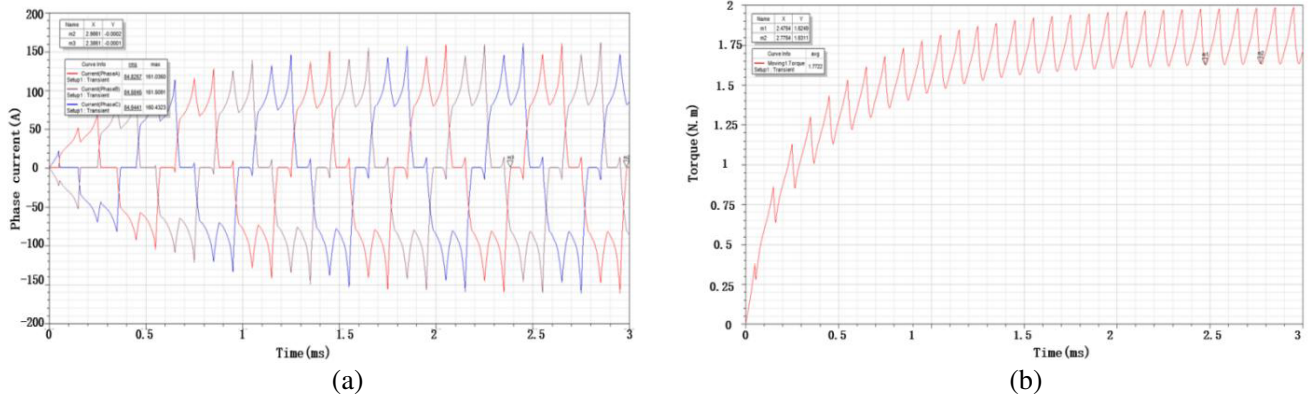


Figure 8. Simulation of magnetic field distribution. (a) Wave of current. (b) Curve of output torque.

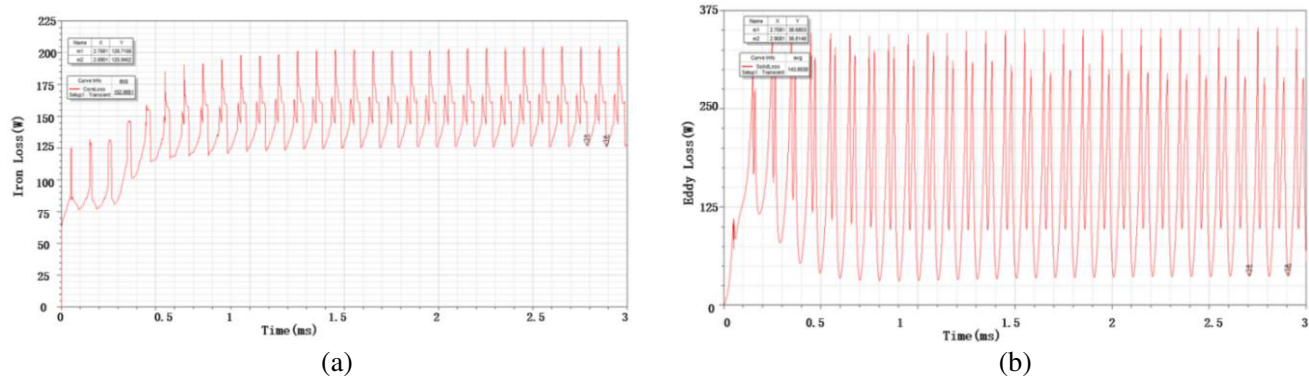


Figure 9. Simulation wave of loss. (a) Iron loss of the motor. (b) Eddy loss of the motor.

5. EXPERIMENT AND VERIFICATION

The experimental prototype has been manufactured as shown in Fig. 10. The test platform was mainly composed of five parts: constant voltage DC power supply cabinet, controller, water supply system, motor, and turbine. Two vibration sensors on the motor body monitor the vibration acceleration at the front bearing and the rear bearing, respectively. The copper loss is tested as shown in Fig. 11. From Fig. 11, it can be seen that the copper loss increases with the increase of rotating speed. The copper loss increases slowly from 20000 to 50000 rpm and rapidly from 50000 to 90000 rpm. At 90000 rpm, the maximum loss is 1.96 W.

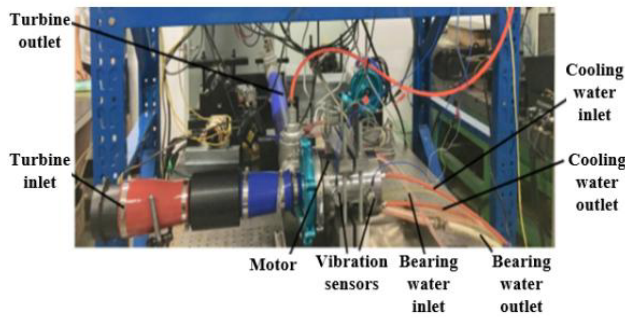


Figure 10. Picture of motor test platform.

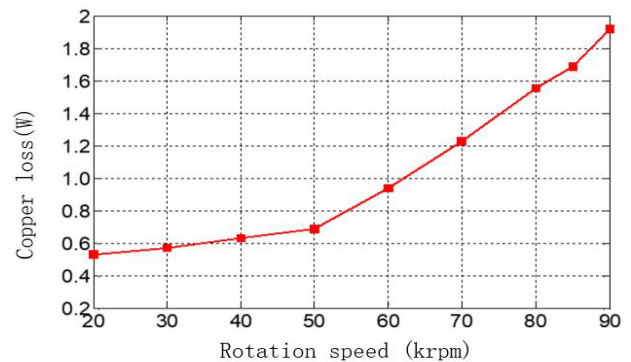


Figure 11. Test result of copper loss.

The electromagnetic efficiency of the motor has been tested under no-load condition. According to the test results, when the speed reached 90000 rpm, the input power of the motor was 1.58 kw, and the electromagnetic power was 1.52 kw. The electromagnetic efficiency of the motor was 96.2%.

6. CONCLUSION

To meet the demand of high power and high rotation speed of air compressor, a motor with 18 kw and 90000 rpm has been designed. This paper focuses on the structural design and loss analysis method of high-speed permanent magnet synchronous motor. The key structural parameters are given. The key structural parameters include PM thickness on loss, outer diameter of stator, air gap length, thickness of yoke, tooth width of stator, and the influence on the loss has been analyzed. Through analysis, it is found that the impact of any of these parameters on these three types of losses is not all in the increasing or increasing trends. Based on the comprehensive consideration of various losses and total losses, the optimized structural parameters are obtained. The analytical and design results are verified by FEM. As shown in the FEM results, the iron loss of the motor is 152 W, and the eddy current loss is 143 W at speed 90000 rpm. The performance of the motor is verified on the prototype test. The electromagnetic efficiency of the motor is 96.2% at speed 90000 rpm. Both of the FEM results and test results on prototype show that the designed motor has good performance.

ACKNOWLEDGMENT

This work was supported by the Fundamental Research Funds for the Central Universities of China under Grant FRF-TP-18-058A1.

REFERENCES

1. Liu, E., L. Lv, Y. Yi, and P. Xie, "Research on the steady operation optimization model of natural gas pipeline considering the combined operation of air coolers and compressors," *IEEE Access*, Vol. 7, 83251–83265, 2019, doi: 10.1109/ACCESS.2019.2924515.
2. Snoussi, J., S. B. Elghali, M. Benbouzid, and M. F. Mimouni, "Optimal sizing of energy storage systems using frequency-separation-based energy management for fuel cell hybrid electric vehicles," *IEEE Trans. Veh. Technol.*, Vol. 67, No. 10, 9337–9346, Oct. 2018.
3. Kim, H. J., J. S. Jeong, M. H. Yoon, J. W. Moon, and J. P. Hong, "Simple size determination of permanent-magnet synchronous machines," *IEEE Transactions on Industrial Electronics*, Vol. 64, No. 10, 7972–7983, Oct. 2017.
4. Lim, M. S., S. H. Chai, J. S. Yang, and J. P. Hong, "Design and verification of 150-krpm PMSM based on experiment results of prototype," *IEEE Transactions on Industrial Electronics*, Vol. 62, No. 12, 7827–7836, Dec. 2015.
5. Zhang, F., R. Dai, G. Liu, and T. Cui, "Design of HSIPMM based on multiphysics fields," *IET Electric Power Appl.*, Vol. 12, No. 8, 1098–1103, Sep. 2018.
6. Pfister, P. D. and Y. Perriard, "Very-high-speed slotless permanent-magnet motors: Analytical modeling, optimization, design, and torque measurement methods," *IEEE Transactions on Industrial Electronics*, Vol. 57, No. 1, 296–303, Jan. 2010.
7. Sun, X., Z. Shi, Y. Cai, G. Lei, Y. Guo, and J. Zhu, "Driving-cycle-oriented design optimization of a permanent magnet hub motor drive system for a four-wheel-drive electric vehicle," *IEEE Trans. Transp. Electrific.*, Vol. 6, No. 3, 1115–1125, Sep. 2020.
8. Sun, X., M. Wu, G. Lei, Y. Guo, and J. Zhu, "An improved model predictive current control for PMSM drives based on current track circle," *IEEE Transactions on Industrial Electronics*, Vol. 68, No. 5, 3782–3793, May 2021, doi: 10.1109/TIE.2020.2984433.
9. Sun, X., Z. Shi, G. Lei, Y. Guo, and J. Zhu, "Multi-objective design optimization of an IPMSM based on multilevel strategy," *IEEE Transactions on Industrial Electronics*, Vol. 68, No. 1, 139–148, Jan. 2021, doi: 10.1109/TIE.2020.2965463.

10. Sun, X., Z. Shi, and J. Zhu, "Multiobjective design optimization of an IPMSM for EVs based on fuzzy method and sequential taguchi method," *IEEE Transactions on Industrial Electronics*, Vol. 68, No. 11, 10592–10600, Nov. 2021, doi: 10.1109/TIE.2020.3031534.
11. Ahmed, S., D. Tremelling, H. Kim, Z. Zhang, N. Frank, and R. McElveen, "Modeling, simulation and performance evaluation of cage rotor permanent magnet motor fed by variable speed drive," *2016 IEEE Energy Conversion Congress and Exposition (ECCE)*, 1–6, 2016, doi: 10.1109/ECCE.2016.7855267.
12. Zhou, Y., L. Zhou, B. Hu, et al., "Design and performance analysis of permanent magnet flux-switching motors using segmental permanent magnets," *IEICE Electronics Express*, Vol. 16, 20190193, 2019.
13. Park, S. H., E.-C. Lee, J.-C. Park, S.-W. Hwang, and M.-S. Lim, "Prediction of mechanical loss for high-power-density PMSM considering eddy current loss of PMs and conductors," *IEEE Transactions on Magnetics*, Vol. 57, No. 2, 1–5, Feb. 2021, Art no. 6300205, doi: 10.1109/TMAG.2020.3007439.
14. Kim, J. H., D. M. Kim, Y.-H. Jung, and M.-S. Lim, "Design of ultra-high-speed motor for FCEV air compressor considering mechanical properties of rotor materials," *IEEE Transactions on Energy Conversion*, Vol. 36, No. 4, 2850–2860, Dec. 2021, doi: 10.1109/TEC.2021.3062646.
15. Mahmoudi, A., S. Kahourzade, N. A. Rahim, and W. P. Hew, "Design, analysis, and prototyping of an axial-flux permanent magnet motor based on genetic algorithm and finite-element analysis," *IEEE Transactions on Magnetics*, Vol. 49, No. 4, 1479–1492, Apr. 2013, doi: 10.1109/TMAG.2012.2228213.
16. Ni, S. and U. Schaefer, "Optimization of a spoke-type permanent magnet motor by combination of genetic algorithm and finite element method," *2018 XIII International Conference on Electrical Machines (ICEM)*, 892–898, 2018, doi: 10.1109/ICELMACH.2018.8506715.
17. Jędrzycka, C., Ł. Knypiński, A. Demenko, and J. K. Sykulski, "Methodology for cage shape optimization of a permanent magnet synchronous motor under line start conditions," *IEEE Transactions on Magnetics*, Vol. 54, No. 3, 1–4, Mar. 2018, Art no. 8102304, doi: 10.1109/TMAG.2017.2764680.
18. Belahcen, A., F. Martin, M. E.-H. Zaim, E. Dlala, and Z. Kolondzovski, "Combined FE and particle swarm algorithm for optimization of high speed PM synchronous machine," *COMPEL-Int. J. Comput. Math. Elect. Electron. Eng.*, Vol. 34, No. 2, 475–484, 2015.
19. Lee, T., M. Seo, Y. Kim, and S. Jung, "Motor design and characteristics comparison of outer-rotor-type BLDC motor and BLAC motor based on numerical analysis," *IEEE Transactions on Applied Superconductivity*, Vol. 26, No. 4, 1–6, Jun. 2016, Art no. 5205506, doi: 10.1109/TASC.2016.2548079.
20. Aliabad, A. D. and F. Ghoroghchian, "Design and analysis of a two-speed line start synchronous motor: Scheme one," *IEEE Transactions on Energy Conversion*, Vol. 31, No. 1, 366–372, Mar. 2016, doi: 10.1109/TEC.2015.2481929.